Journal of Water Process Engineering 82 (2026) 109479

Contents lists available at ScienceDirect

Journal of Water Process Engineering

journal homepage: www.elsevier.com/locate/jwpe

Surface-decorated polyethylene glycol-graphene oxide nanohybrids for fouling mitigation in aminated polysulfone membranes treating oily wastewater

Y. Jafarzadeh [a,b], C. García-Payo [a], M. Khayet [a,c,*]

[a] Department of Structure of Matter, Thermal Physics and Electronics, Faculty of Physics, University Complutense of Madrid, Avda. Complutense s/n, 28040, Madrid, Spain
[b] Faculty of Chemical Engineering, Sahand University of Technology, Tabriz, Iran
[c] Madrid Institute for Advanced Studies of Water (IMDEA Water Institute), Avda. Punto Com, N° 2, 28805, Alcalá de Henares, Madrid, Spain

ARTICLE INFO

Editor: Tzyy Haur Chong

Keywords:
Oily wastewater
Graphene oxide
Polysulfone membrane
Amination
Reduced fouling

ABSTRACT

Membrane fouling remains a critical challenge in oily wastewater treatment, limiting the efficiency of conventional polymeric membranes. Graphene oxide (GO) is a promising hydrophilic modifier, but its tendency to restack restricts interlayer spacing and limits antifouling performance. In this work, we present polyethylene glycol (PEG)-functionalized GO nanosheets, with adjustable molecular weights, to effectively expand GO interlayer spacing and enhance the hydrophilicity and antifouling capabilities of aminated chloromethylated polysulfone (AM-CMPSF) membranes. PSF was first chloromethylated and fabricated via non-solvent induced phase separation method, followed by amination using ethylenediamine to form AM-CMPSF membranes. GO nanosheets were synthesized and functionalized with PEG of varying molecular weights, then stacked onto the membrane surface. XRD analysis confirmed that increasing PEG molecular weight broadened interlayer *d*-spacing between GO nanosheets. The resulting GO-PEG/AM-CMPSF membranes exhibited significantly improved surface hydrophilicity, with rapid water absorption preventing contact angle measurement, and increased water uptake (from 30.6% for the pristine membrane (M0) to 84.6% for GO-PEG20000 (M6)), and pure water flux (from 5.9 to 16.9 $L{\cdot}m^{-2}{\cdot}h^{-1}$). Filtration tests using a 1000 $mg{\cdot}L^{-1}$ oil-in-water emulsion revealed enhanced permeate flux and fouling resistance. All membranes maintained high oil rejection (85.6% - 88.1%). Permeate flux decline decreased from 41.2% for M0 to 27.2% for M6, irreversible fouling ratio from 28.6% to 23.0%, and the flux recovery ratio increased from 71.2% to 87.0%. The results demonstrate that PEG-modified GO effectively enhanced membrane hydrophilicity, antifouling behavior, and filtration performance, offering a promising strategy for advanced oily wastewater treatment.

1. Introduction

Discharged oily wastewater effluents produced from different industries like oil and gas exploration, petrochemical, metallurgical, food, textiles has become a major concern all over the world because of causes various adverse effects on the environment by polluting surface water, underground water, as well as the soil [1–3]. Conventional treatment methods such as physical [4,5] and chemical [6,7] approaches, often struggle to effectively remove fine oil-in-water emulsions, particularly those containing oil droplets with diameters smaller than 20 μm [3].

Membrane separation technology has emerged as an efficient method for treating oil-in-water emulsions and has gaining considerable attention in recent years [6,8–11]. However, its broader application is hindered by membrane fouling [12–14]. Key membrane properties, including hydrophilicity, pore size structure, surface roughness and surface charge, are known to play critical roles in determining membrane fouling propensity [14–17]. Therefore, different strategies have been adopted to mitigate fouling phenomenon including among others membrane surface modification (e.g. interfacial polymerization) [12,18], incorporation of hydrophilic additives into membrane matrix [19–22], blending with hydrophilic polymers [13,23–25], and assembling of two-dimensional nanosheets on the membrane [26–28].

* Corresponding author at: Department of Structure of Matter, Thermal Physics and Electronics, Faculty of Physics, University Complutense of Madrid, Avda. Complutense s/n, 28040, Madrid, Spain.
E-mail address: khayetm@fis.ucm.es (M. Khayet).

https://doi.org/10.1016/j.jwpe.2026.109479
Received 30 October 2025; Received in revised form 14 December 2025; Accepted 7 January 2026
Available online 15 January 2026

As a typical polymer used in membrane fabrication, polysulfone (PSF) is one of the most widely used commercial materials in industrial production of microfiltration/ultrafiltration membranes due to applicability in wide range of pH, its excellent tensile strength, high filtration capability, chemical resistance and thermal stability [29,30]. Nevertheless, one of the biggest challenges is to improve the performance and fouling resistance of PSF membranes due to its hydrophobicity, resulting in increased foulant's adsorption into their surfaces [4,8,14]. Extensive research efforts have been undertaken to enhance the performance of PSF-based membranes for water treatment [9,29,31–33]. Importantly, using salt-containing coagulation baths during phase inversion has a significant impact on PSF membrane morphology and performance. The presence of salts in the coagulation bath alters demixing kinetics, pore size distribution, and surface hydrophilicity, thereby affecting permeate flux, oil rejection, and fouling resistance. For example, Alias et al. [34] demonstrated that incorporating monovalent (NaCl, KCl) and divalent (Na_2SO_4) salts into the coagulation bath significantly influences phase separation kinetics and PSF membrane morphology, enabling controlled pore structure formation and improved separation performance. Similarly, incorporating functional additives such as sodium acrylate-based polymers into the coagulation bath, enhanced hydrophilicity and oleophobicity, reducing fouling and improving durability [35]. These findings underscore that a salt-containing coagulation bath is not merely an auxiliary condition but a key design parameter that critically influences membrane performance.

Recent mitigation strategies on membrane fouling have been demonstrated in designing various membranes with high antifouling properties by synthesized or commercial membranes via surface coating and surface grafting techniques [14,29]. Most researchers use hydrophilic materials to prevent foulants from attaching to the modified membrane surface [29,36–38].

Assembling 2D nanosheets on membrane surface has attracted much attention during last decade due to the easy of some applied fabrication procedures and the outstanding characteristics of 2D nanosheets such as graphene oxide (GO) [39,40]. This is a unique material consisting of sheets of carbon atoms arranged in a honeycomb lattice and decorated with various oxygen-containing functional groups such as hydroxyl, carboxyl, carbonyl and epoxy [20,28,41,42]. GO has been widely used in different membrane separation processes due to its excellent physicochemical properties, high surface area, high mechanical and chemical stability, antifouling and hydrophilic properties and easy fabrication [39,43–46]. In addition, GO is single-atom-thick, which makes it stackable allowing for the preparation of ultra-thin membranes with minimal mass transport resistance [47–49]. When stacked over a polymeric membrane support, water molecules zigzag through the nanochannels between GO layers due to the capillary effect while solutes are rejected [28]. Different kinds of functionalized GO have been reported with improved flux, rejection and resistance to fouling [50–53]. Incorporating hydrophilic functional groups (such as amine groups) can be an effective way to reduce the PSF membrane hydrophobicity and improve its permeation flux and its anti-fouling properties. Alkhouzaam et al. [50] prepared PSF composite membranes by incorporating polydopamine-functionalized GO particles (rGO-PDA). The enhancement of hydrophilicity and surface roughness resulted in a high pure water flux, approximately 1.8 times higher than the pristine PSF without affecting the rejection performance. Yasir et al. [52] prepared PSF membranes incorporating GO functionalized with poly(amido amine) (PAMAM) which exhibited 22-fold enhancement water permeation flux and 99% oil rejection. Abdalla et al. [53] reported an increase of 97% in water permeability and oil rejection reached 97.9% at 0.2 wt% of aspartic acid (AA) functionalized GO loading in PSF composite membranes compared to pristine PSF membrane due to the presence amine groups in GO functionalized with AA. In parallel, chemical modification of the PSF backbone has also been investigated as a strategy to overcome its inherent hydrophobicity [29,54–56]. The addition of functional groups into the PSF backbone not only mitigates the hydrophilic and antifouling limitations of the pristine PSF, but also introduces tunable functionalities, broadening both structural versatility and application scope. Chloromethylation reactions have been adopted by researchers as valuable strategies to generate reactive groups in the polymer chain that can be further functionalized by the easy substitution of the chloromethyl groups with aldehyde, ester, amine or quaternary ammonium groups, among others [56].

Despite extensive studies on PSF membrane modification for oily wastewater treatment, most studies have focused on either surface or bulk modification strategies. Such single-modification approaches often enhance only one performance parameter, such as permeate flux or oil rejection, while rarely achieving simultaneous improvements in flux, rejection, and fouling resistance. This limitation underscores the need for a synergistic approach that integrates backbone functionalization with advanced nanosheet assembly, while carefully optimizing fabrication conditions.

In this study, we present a novel approach to stack both unmodified and modified GO layers onto aminated PSF membranes. PSF was aminated to improve compatibility with GO nanosheets by introducing reactive amine groups, thereby strengthening interfacial bonding and mechanical stability. This modification was carried out in two steps. First, PSF was chloromethylated to facilitate interaction with amine groups, and the resulting chloromethylated PSF (CMPSF) membranes were prepared via the non-solvent induced phase separation (NIPS) method. Subsequently, the CMPSF membranes were aminated by ethylenediamine to obtain aminated PSF (AM-CMPSF) membranes. Concurrently, GO was functionalized with PEG to increase hydrophilicity, optimize interfacial interactions, and reduce fouling during oil–water separation. Finally, both pristine and PEG-modified GO were stacked on the AM-CMPSF membranes. All prepared membranes were then characterized and evaluated for oil-in-water emulsion separation.

2. Materials and methods

2.1. Materials

Polysulfone (PSF; weight-average molecular weight ~ 60,000 $g{\cdot}mol^{-1}$) supplied by Acros Organics was used. Chloroform (purity: 99.8%), paraformaldehyde (purity: 95%), trimethylchlorosilane (purity: 98%), stannic chloride (purity: 98%), 1-methyl-2-pyrrolidone (NMP; purity: 99%), N,N′-dicyclohexylcarbodiimide (DCC; purity: 99%), 4-(dimethylamino) pyridine (DMAP; purity: 99%), N, N-dimethylformamide (DMF; purity: 99.8%), graphite (purity: 98%), potassium permanganate (purity: 99%), ethanol (purity: 99.8%), methanol (purity: 99.8%), hydrogen peroxide aqueous (purity: 30%), sulfuric acid (purity: 98%), hydrochloric acid (purity: 37%), polyethylene glycol (weight-average molecular weight = 1000, 6000 and 20,000 $g{\cdot}mol^{-1}$), ethylenediamine (EDA; purity: 99%) and sodium dodecyl sulfate (SDS; purity: 99%) were purchased from Sigma-Aldrich. All materials were used as received.

2.2. Synthesis of GO and GO-PEG

GO nanosheets were synthesized via a modified Hummers method as described elsewhere [26,57]. First, 5.0 g of graphite was mixed with 190 mL of sulfuric acid and stirred for 30 min in an ice bath. Then, 25.0 g of potassium permanganate was added to the solution and stirred for 12 h at 35 °C. Subsequently, 250 mL of distilled (DI) water was added dropwise to the reaction mixture under continuous stirring in an ice bath. The suspension was then transferred to a beaker and further diluted with 1 L of DI water. To terminate the oxidation reaction, hydrogen peroxide was added dropwise, followed by stirring for 30 min. The resulting dispersion was vacuum filtrated using a filter paper and washed with 2 L of hydrochloric acid aqueous solution to remove the remained chemicals. Finally, it repeatedly rinsed with DI water, and the obtained GO was recovered by freeze-drying. PEG was decorated onto

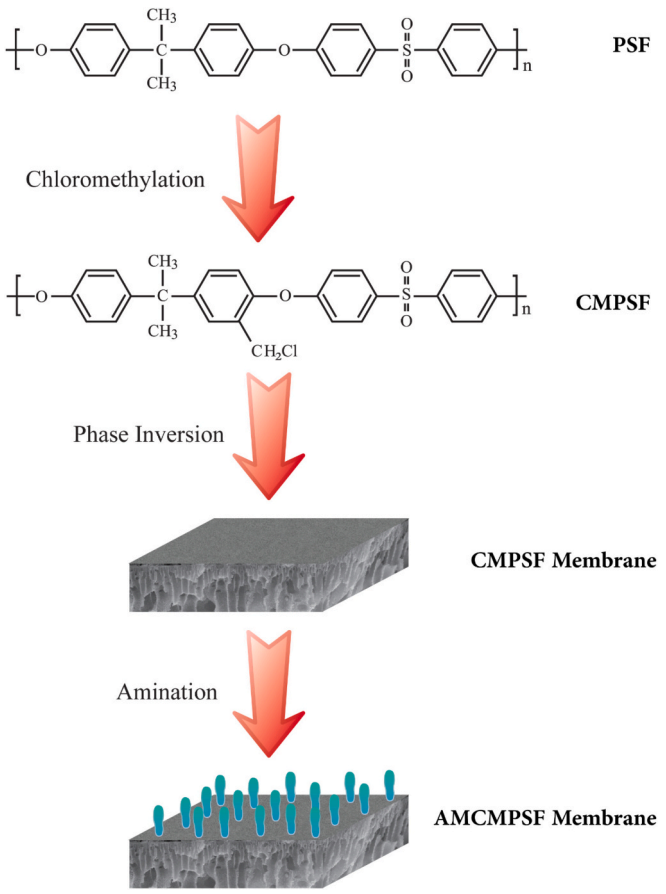

Fig. 1. Schematic illustration of CMPSF synthesis, CMPSF membrane fabrication, and subsequent amination to produce the AM-CMPSF membrane.

the prepared GO according to the procedure described by Mohammadi et al. [58]. Briefly, 100 mg of GO was dispersed in 100 mL of DI water and then 1000 mg of PEG was added to the suspension and was vigorously stirred at room temperature. Separately, 400 mg of DCC and 100 mg of DMAP were dissolved in 40 mL of DMF and pre-stirred for 30 min. This resulting solution was subsequently added to the GO-PEG suspension, and the reaction mixture was stirred for 48 h to allow the coupling reaction to proceed. The GO-PEG was finally precipitated by adding 200 mL of methanol, washed thoroughly with DI water, and centrifuged. In this study, three types of GO-PEG nanosheets were synthesized using PEG with different molecular weights (1000, 6000 and 20,000 g·mol^{-1}), hereafter referred to as GO-PEG-1000, GO-PEG-6000 and GO-PEG-20000, respectively.

2.3. Chloromethylation of PSF

Chloromethylated PSF (CMPSF) was synthesized following a previously reported procedure [59–61]. Briefly, 10 g of PSF was dissolved in 500 mL of chloroform under continuous stirring in a three-necked flask equipped with a reflux condenser to obtain a homogenous solution. Subsequently, 6.78 g of paraformaldehyde and 24.6 g of trimethylchlorosilane were added into the solution, followed by the dropwise addition of 1.178 g of stannic chloride. The reaction mixture was then maintained at 52 °C for 48 h. Upon pouring the reaction mixture into an ethanol bath, a white flocculent precipitate was formed, which was repeatedly washed with ethanol and DI water, filtered, and dried in an oven at 50 °C for 24 h. The degree of chloromethylation (*DC*) of CMPSF was calculated using the following equation [33,62,63]:

Table 1
Membrane codes prepared in the present study. PSF: polysulfone, CMPSF: chloromethylated polysulfone, AM-CMPSF: aminated-chloromethylated polysulfone, PEG100, PEG6000 and PEG20000: PEG molecular weight 1000, 6000 and 20,000 g·mol^{-1}, respectively.

Membrane	Polymer layer	GO or GO-PEG layer
M0	PSF	–
M1	CMPSF	–
M2	AM-CMPSF	–
M3	AM-CMPSF	GO
M4	AM-CMPSF	GO-PEG1000
M5	AM-CMPSF	GO-PEG6000
M6	AM-CMPSF	GO-PEG20000

$$DC = \frac{3B}{A} \quad (1)$$

where *A* and *B* are the integrated areas of signals at 1.72 ppm and 4.56 ppm in the ^{1}H NMR spectrum of CMPSF, respectively.

2.4. Preparation of PSF and CMPSF membranes

PSF and CMPSF membranes were prepared using non-solvent induced phase separation (NIPS) method. Solutions containing 14 wt% polymer (PSF or CMPSF) and 86 wt% NMP were prepared and stirred at 48 °C for at least 10 h until clear homogeneous solutions were obtained. The casting solutions were then degassed for 24 h to remove entrapped air bubbles. Subsequently, the dope solutions were cast on a flat glass plate using an automatic casting knife (Elcometer 4340, Elcometer Limited, UK) to form flat-sheet membranes. The cast films were immediately immersed in a DI water coagulation bath for 24 h to induce phase separation. Finally, the prepared membranes were dried at room temperature prior to characterization.

2.5. Amination of CMPSF membranes

CMPSF membranes were immersed in a 5 M EDA solution at 27 °C for 20 min. This duration was selected because longer immersion caused membrane deformation and shrinkage, while shorter immersion resulted in insufficient amination, preventing proper stacking of the GO layers on the resultant membranes. The resulting AM-CMPSF membranes were subsequently washed with methanol and DI water, followed by drying overnight. The schematic representation of the followed procedure was shown in Fig. 1.

2.6. Deposition of GO and GO-PEG layers on AM-CMPSF membranes

After the preparation of AM-CMPSF membranes, different GO and GO–PEG layers were deposited onto their functionalized surface. GO or GO-PEG powders were first dispersed in DI water by probe sonication (Fisherbrand™ Sonicador Q500) for 15 min until a homogeneous suspension was obtained. The concentration of all suspensions was adjusted to 1000 mg·L^{-1}. Finally, the suspensions were stacked onto the AM-CMPSF membranes under vacuum pressure of 0.65 bar at 27 °C, followed by drying at room temperature.

In this study, seven membranes were prepared and labeled hereafter as M0, M1, M2, M3, M4, M5 and M6 as summarized in Table 1.

2.7. Characterization

To confirm the chloromethylation of PSF, the ^{1}H NMR spectrum of CMPSF was obtained from a Bruker AV 400 MHz Wide Bore spectrometer with $CDCl_3$ employed as solvent. Fourier transform infrared spectroscopy (FTIR) analysis was used to investigate characteristic peaks of membranes using a Nicolet device (Magna-IR 750 Series II) equipped with a detector DTGS-KBr (sulfate triglycerin deuterated with KBr

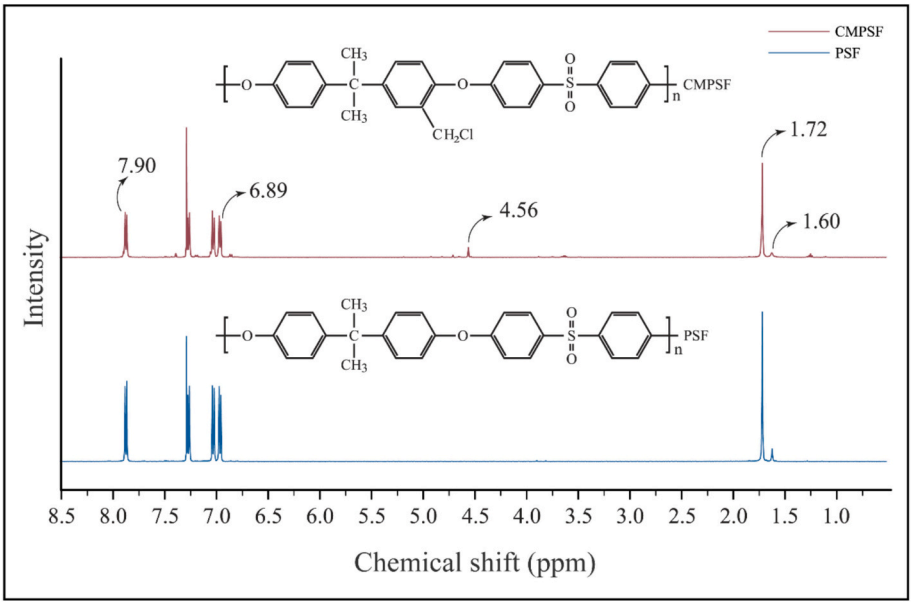

Fig. 2. ^{1}H NMR spectra of PSF and CMPSF.

window), a beam splitter KBr and an infrared source (Ever-Glo). The H-ATR Multiple Bounce (Spectra Tech) accessory with a ZnSe crystal and 13 steps was used for analysis. ATR-FTIR measurements were carried out in the range of 500–4000 cm^{-1} at 128 scans and 8 cm^{-1} resolution. The morphological structure of the cross-section of all membranes was studied by FESEM (FESEM; MIRA3 FEG-SEM, Tescan Co., Czech). Dried samples were fractured in liquid nitrogen and then coated with gold by sputtering (Q150RS, Quorum). X-ray diffraction analysis (PW1730, Philips) was performed to study the crystalline structure of the prepared membranes in the scanning range of 2θ between 5° and 60°. The water contact angles (*WCA*) of the membrane surfaces were measured using both static and dynamic methods via a PGX Pocket Goniometer (TQC Sheen, Industrial Physics, USA). For the static measurements, five droplets were considered for each membrane, and the average value was reported as the static contact angle. For the dynamic measurements, advancing and receding angles were obtained by monitoring changes in droplet volume over time. Mechanical strength of membranes was measured by a tensile testing machine (STAM-D, SANTAM, Iran). All samples were cut in rectangular shape, and the testing speed was adjusted at 10 $mm{\cdot}min^{-1}$. Each membrane was tested at least 3 times and averaged values were reported. The water uptake (*WU*) of the membranes was determined by weighing both dry and hydrated samples. Small sections of each membrane were cut and dried overnight, after which they were weighed and immersed in deionized (DI) water for 30 min. Excess water on the membrane surface was then gently removed, and the wet membranes were weighed again. The *WU* value of each membrane was calculated using the following equation [38]:

$$WU\ (\%) = \left(\frac{m_w - m_d}{m_w}\right) \times 100 \tag{2}$$

where m_w and m_d are the weights of the wet and dry membrane, respectively.

2.8. Filtration experiments

The microfiltration performance of the prepared membranes was evaluated in a lab-scale crossflow filtration system described elsewhere [64]. Prior to the measurements, the membranes were compacted for at least 60 min under a transmembrane pressure (*TMP*) of 3 bar using DI water as feed until a stable permeate flux was achieved. The TMP was determined from Eq. (3):

$$TMP = \left(\frac{P_f + P_r}{2} - P_p\right) \tag{3}$$

where P_f, P_r and P_p are the upstream (feed), downstream (retentate) and permeate pressure in the cross-flow module cell expressed in bar, respectively. The upstream and downstream pressures were measured using absolute pressure gauges positioned immediately before and after the membrane module, respectively. The permeate side was maintained at atmospheric pressure.

After that, DI water permeate flux $(J_{w,0})$ was measured at a *TMP* of 1.5 bar. Subsequently, the feed tank was filled with an oil-in-water emulsion, which was previously prepared by dispersing 5000 mg of vegetable oil and 25 mg of SDS in 5 L of DI water at 1500 rpm for 24 h. This oil/water emulsion concentration (1000 $mg{\cdot}L^{-1}$) is typically concentration of oil in water generated from oil and gas reservoirs in oilfields [38]. The permeate flux was measured by weighing every 15 min over a period of 4 h and calculated using the following equation

$$J = \frac{m}{A.\Delta t} \tag{4}$$

where m is the permeate mass collected over a time interval (Δt) and A is the effective membrane area (21.76 ± 0.01 cm^2). After a certain time, permeate flux decline (*FD*) occurred due to fouling process and it can be calculated as:

$$FD_{oil}(\%) = \left(1 - \frac{J_{oil,t}}{J_{oil,0}}\right) \times 100 \tag{5}$$

where $J_{oil,t}$ is the final (or stable) permeate flux of the membrane at t time ($L/m^{-2}\ h^{-1}$) at 4 h in our study, and $J_{oil,0}$ is the initial permeate flux.

The oil rejection was calculated by determining the oil concentration in the feed, retentate and permeate streams by turbidity measurements (HF Micro 100 turbidimeter). The oil rejection factor, R, was calculated by the following equation [12]:

$$R(\%) = \left(1 - \frac{2C_p}{C_r + C_f}\right) \times 100 \tag{6}$$

where C_p, C_r and C_f are the oil concentrations in the permeate, retentate and feed streams, respectively.

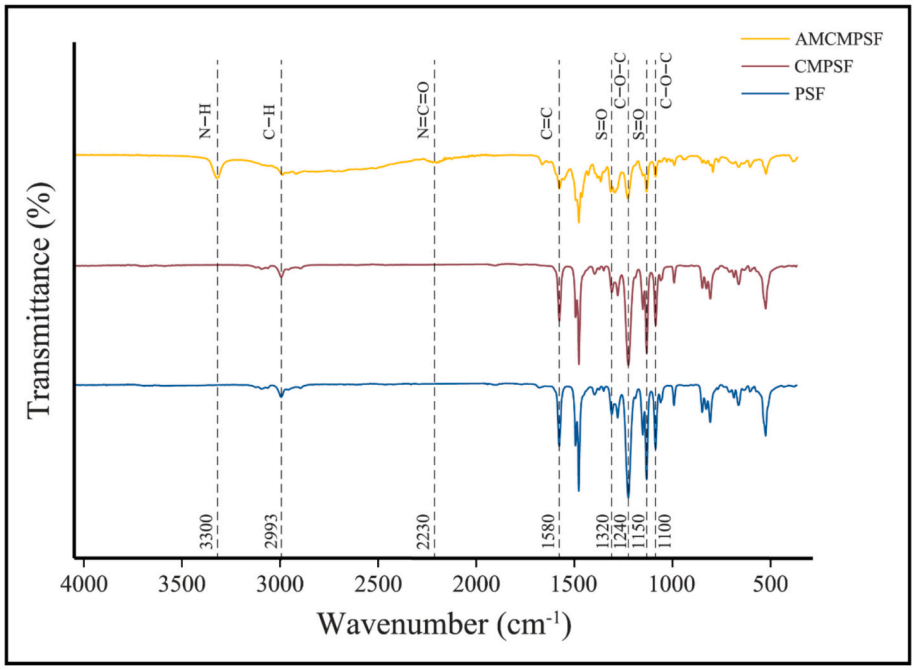

Fig. 3. ATR-FTIR spectra of PSF, CMPSF and AM-CMPSF membranes.

To evaluate the oil-fouling resistance of the membranes, the feed tank was subsequently emptied and thoroughly rinsed multiple times, then refilled with DI water. The DI water permeate flux was measured again after fouling $(J_{w,1})$. The flux recovery ratio (*FRR*) was calculated according to the following equation to assess the antifouling performance of the membranes in terms of pure water reduction [31,65]:

$$FRR(\%) = \frac{J_{w,1}}{J_{w,0}} \times 100 \tag{7}$$

Additionally, the oil-water relative flux reduction (*RFR*) was also determined as:

$$RFR(\%) = \left(1 - \frac{J_{oil,t}}{J_{w,0}}\right) \times 100 \tag{8}$$

3. Results and discussion

3.1. Chloromethylation of PSF and amination of CMPSF membrane

The ^{1}H NMR spectra of both PSF and CMPSF are shown in Fig. 2. As can be seen in both spectra, the signals observed at 1.60–1.72 ppm correspond to the six hydrogen in the methyl groups [55,66], whereas the signals that appeared in the 6.89–7.90 ppm range can be attributed to the two hydrogen of the phenyl groups [67]. Notably, a new signal at approximately 4.56 ppm is observed in the CMPSF spectrum, which is assigned to hydrogens in benzyl chloride (CH_2Cl and HC) [59,61], confirming the successful chloromethylation of PSF. The degree of chloromethylation, estimated using Eq. (1) was found to be 21%. This value was selected based on preliminary optimization experiments, which showed that higher substitution levels (> 25%) caused excessive rigidity and poor membrane processability, while lower levels (< 15%) resulted in insufficient reactive sites for effective amination. At 21%, the PSF backbone maintains adequate mechanical flexibility while providing enough chloromethyl groups to facilitate amination [33,63]. This balance was found to be optimal for producing membranes with enhanced mechanical stability and improved compatibility with GO nanosheets.

ATR-FTIR spectroscopy was employed to investigate the functional group modifications in PSF, CMPSF and AM-CMPSF membranes (Fig. 3).

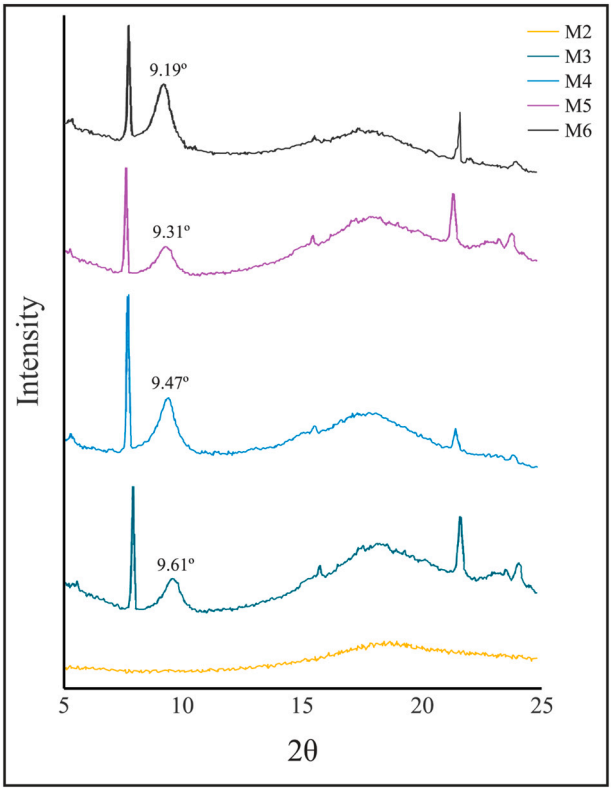

Fig. 4. XRD spectra of AM-CMPSF (M2) GO/AM-CMPSF (M3) and GO-PEG/AM-CMPSF membranes with different PEG molecular weights (M4, M5, and M6).

The successful chloromethylation of PSF was qualitatively confirmed by ATR-FTIR, as evidenced by the appearance of a peak at 2993 cm^{-1}, corresponding to the stretching vibrations of the methylene (CH_2) groups. Amination of the CMPSF membranes was achieved via reaction with ethylenediamine under moderate reaction condition. The AM-

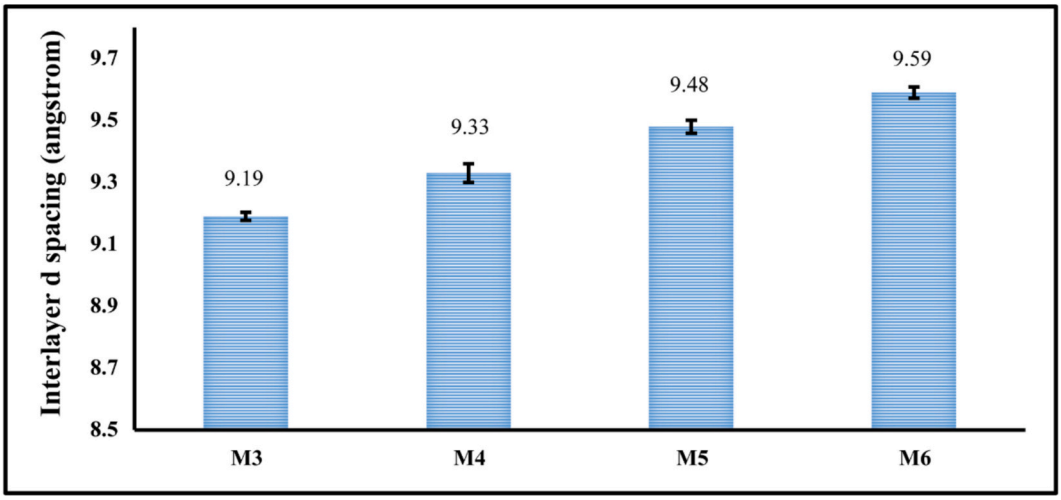

Fig. 5. Interlayer *d*-spacing of GO (M3) and GO-PEG (M4, M5, and M6) stacked on the AM-CMPSF membrane surfaces.

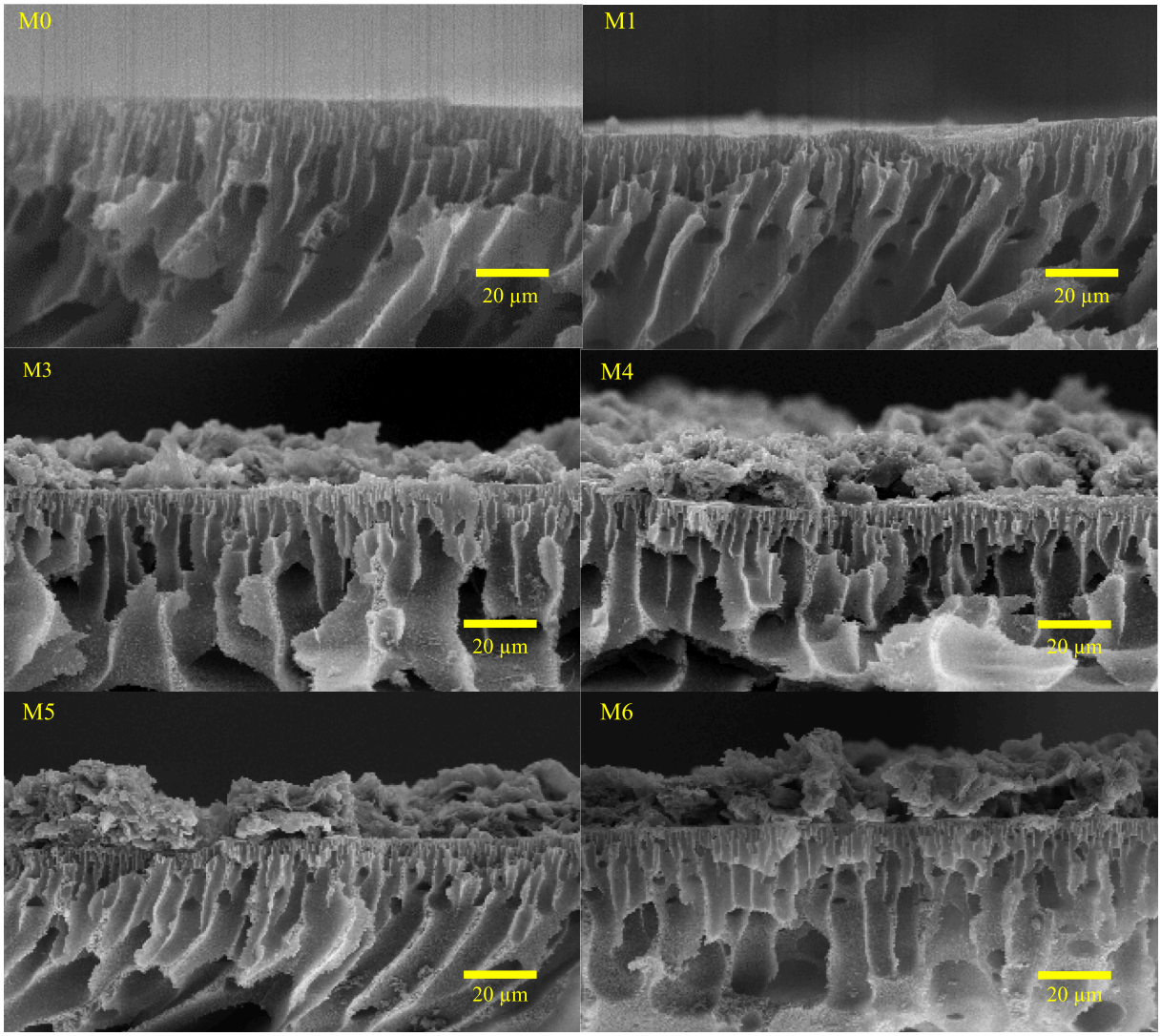

Fig. 6. Cross-sectional FESEM images of pristine PSF (M0), CMPSF (M1), GO/AM-CMPSF (M3) and GO-PEG/AM-CMPSF with different PEG molecular weights (M4, M5 and M6) membranes. The FESEM image of AM-CMPSF (M2) membrane is not shown, as its morphology is similar to that of M1.

CMPSF membrane not only provides suitable ligand sites for subsequent GO-PEG functionalization but also introduces amino groups on the PSF backbone, enabling further partial crosslinking with unreacted chloromethyl groups [66]. The formation of amino functionalities in AM-

Table 2
Membrane characteristics: thickness (δ), water contact angle (*WCA*); water uptake (*WU*), tensile strength and elongation at break.

Membrane	δ (μm)	Static WCA (°)	*WU* (%)	Tensile strength (MPa)	Elongation at break (%)
M0	108 ± 11	85.2 ± 1.3	30.6 ± 3.7	5.12 ± 0.21	26.4 ± 2.7
M1	99 ± 7	74.7 ± 1.6	32.1 ± 2.2	4.9 ± 0.3	31.7 ± 1.9
M2	102 ± 14	69.8 ± 2.1	36.8 ± 4.1	5.1 ± 0.3	28.5 ± 3.5
M3	123 ± 16	NM[a]	64.9 ± 6.9	6.43 ± 0.14	14.3 ± 1.0
M4	119 ± 9	NM	72.0 ± 5.2	6.38 ± 0.28	14.0 ± 1.4
M5	127 ± 12	NM	77.4 ± 4.8	6.51 ± 0.21	13.8 ± 1.1
M6	136 ± 7	NM	84.6 ± 3.7	6.55 ± 0.18	13.5 ± 1.5

[a] WCA was not measured (NM) because of the rapid adsorption of water-droplets on the membrane surface. To illustrate this behavior, a video demonstrating the rapid adsorption of a water droplet on the surface ofthe membrane M3 has been recorded and provided as Supplementary data.

CMPSF membranes was confirmed by the ATR-FTIR peaks at ~1600 cm^{-1}, which is attributed to (N—H bending), and a broad peak at 3300 cm^{-1} corresponding to the N—H stretching [68], indicating the successful incorporation of -NH_2 groups on the CMPSF membrane surface.

3.2. Membrane characterization

Fig. 4 shows the XRD spectra of AM-CMPSF (M2), GO/AM-CMPSF (M3), and GO-PEG/AM-CMPSF membranes with different PEG molecular weights (M4, M5, M6). The interlayer *d*-spacing of GO nanosheets of these membranes was calculated using Bragg's law:

$$d = \frac{\lambda}{2sin\theta} \quad (9)$$

and the results were depicted in Fig. 5. The M3 membrane containing pristine GO layer exhibited a peak at $2\theta = 9.61°$ corresponding to an interlayer *d*-spacing of 0.920 nm. After GO decoration with PEG, the characteristic GO peak shifted slightly to lower 2θ values depending on the PEG molecular weight (i.e. higher PEG molecular weights resulted in smaller shifts of the characteristic peak).

In Fig. 4, the characteristic GO peaks for membranes M3, M4, M5 and M6 appeared at 2θ values of 9.61°, 9.47°, 9.31° and 9.19°, respectively. These results indicate that modification of GO with higher molecular weight PEG leads to increased interlayer *d*-spacing of the GO nanosheets (Fig. 5), demonstrating a direct correlation between the interlayer *d*-spacing and the PEG molecular weight. As previously discussed, water molecules can permeate through the GO nanosheets via a zigzag pathway facilitated by capillary effects, whereas oil droplets are effectively rejected [27,28]. Although the increase in interlayer *d*-spacing due to PEG incorporation was modest (i.e. 4.35% from M3 to M6), it is sufficient to enhance water permeation through the GO layer while maintaining rejection of larger oil droplets.

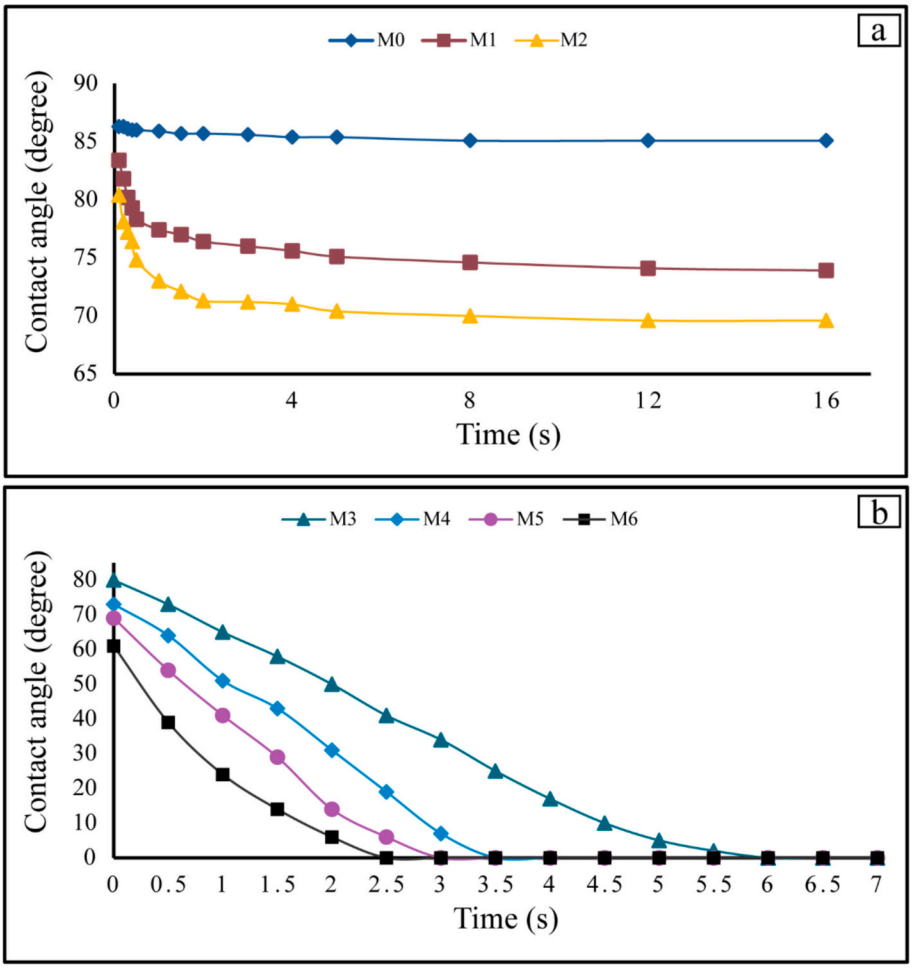

Fig. 7. Dynamic contact angles of the prepared membranes: (a) M0, M1, and M2; and (b) M3, M4, M5 and M6, showing the rapid droplet adsorption on the GO and GO-PEG layers of the membranes.

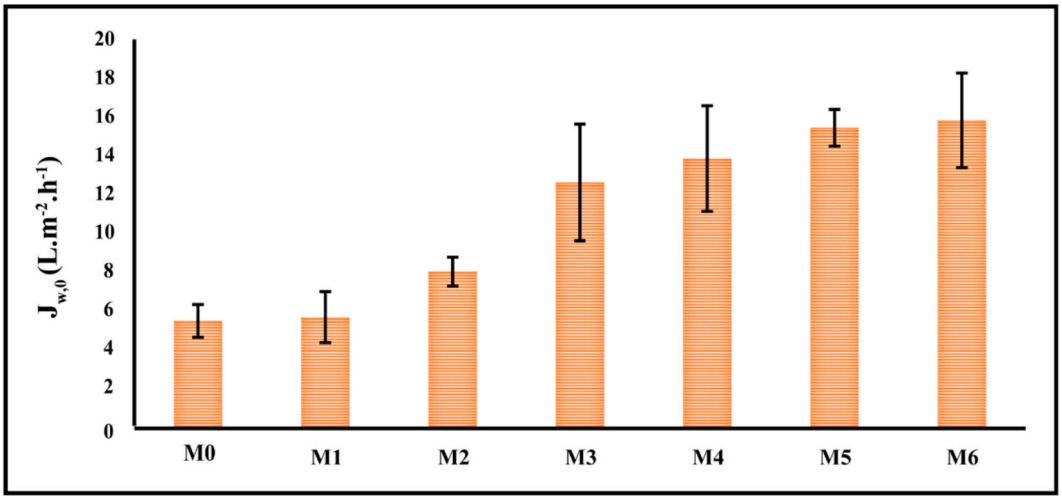

Fig. 8. Pure water flux of the pristine PSF membrane (M0), CMPSF membrane (M1), AM-CMPSF membrane (M2), GO stacked AM-CMPSF membrane (M3) and GO-PEG stacked AM-CMPSF membranes (M4, M5 and M6).

The cross-sectional FESEM images of all prepared membranes are given in Fig. 6. All membranes exhibit a characteristic asymmetric structure, comprising a thin selective top layer, an underlying finger-like layer, and a bottom layer with macro-voids, which is characteristic of membranes prepared via the NIPS method [30,69,70]. No significant differences were observed between the cross-section of the pristine PSF membrane (M0) and the CMPSF layer in the modified membranes. However, the thickness of the GO layer deposited on the top surface of AM-CMPSF membranes increased as the molecular weight of PEG was increased. This is witnessed through the XRD results as discussed previously.

The hydrophilic properties of the membranes were evaluated by static water contact angle (WCA) and water uptake (WU), and the results are summarized in Table 2. Additionally, the dynamic contact angles of the prepared membranes are shown in Fig. 7, providing a more accurate and reliable assessment of membrane wettability. The pristine PSF membrane (M0) exhibited a WU of 30.6%, which increased to 32.1% and 36.8% for the CMPSF (M1) and AM-CMPSF (M2) membranes, respectively. This trend is consistent with the reduction in WCA from 85.2°, (M0) to 74.7° (M1) and 69.8° (M2), as can be seen in Table 2, confirming that chloromethylation of PSF followed by amination introduces hydrophilic functional groups that enhance water affinity. In addition, membranes without GO or GO-PEG layers (M0–M2) displayed lower *WU* values compared to GO-containing membranes (M3–M6), due to the additional hydrophilic functional groups in both GO and GO-PEG layers. Furthermore, incorporation of PEG between GO nanosheets further increased *WU*, with higher PEG molecular weight yielding greater water affinity. This effect is attributed to both the hydrophilic nature of PEG and the expanded interlayer *d*-spacing of GO induced by PEG decoration, as discussed previously. Consequently, PEG functionalization is expected to enhance water permeate flux without compromising oil rejection. It should be noted that WCA measurements could not be obtained for GO and GO-PEG stacked membranes due to rapid water absorption, indicating their superhydrophilic character. The dynamic contact angle measurements (Fig. 7b) further support this observation, with both advancing and receding angles rapidly approaching zero, indicating complete wetting.

The mechanical properties of the fabricated membranes are also listed in Table 2. As can be seen, generally the membranes without a GO layer (M0, M1, and M2) exhibited tensile strengths of approximately 5 MPa, whereas the incorporation of a GO layer increased this value to ~6.5 MPa. However, the elongation at break decreased by nearly 50% in the presence of GO layers on the membrane surface compared to M2 membrane. The improvement in tensile strength of the thin-film composite membranes can be attributed to strong interfacial interactions between polymer matrix and GO/GO-PEG layers, which restrict the mobility of the polymer backbone and enhance structural rigidity.

The GO and GO-PEG layers can establish strong interfacial interactions with the AM-CMPSF surface, including hydrogen bonding and π–π stacking. These interactions restrict polymer chain mobility, enhancing load transfer efficiency under stress [71] and resulting in increased tensile strength. However, the same restriction of chain mobility limits the polymer matrix's capacity for plastic deformation. Due to the rigid and planar structure, GO nanosheets can react to localized stress concentrations, which limit membrane elongation. Consequently, the membranes become stiffer and more brittle, as reflected by the ~50% reduction in elongation at break compared to the membrane M2. This demonstrates that the modification strategy enhances mechanical robustness without compromising practical usability. Overall, the incorporation of GO and GO-PEG layers improves the structural integrity of the membranes by increasing tensile strength, while the reduction in elongation reflects the expected stiffening effect [72]. This balance of mechanical properties confirms that the resulting membranes are mechanically reliable for practical water treatment applications.

3.3. Performance evaluation of membranes

Both the morphological structure and hydrophilic character of the membrane strongly influence their pure water flux ($J_{w,0}$) and oil rejection performance (R). Fig. 8 presents the pure water flux of the prepared membranes. A significant increase in $J_{w,0}$ was observed upon stacking GO onto the AM-CMPSF, with membrane M3 exhibiting approximately 57% higher pure water flux, compared to M2. This improvement can be mainly attributed to the unique water transport properties of GO nanochannels, as previously reported [27,28,73]. In addition, the direct correlation between J_w values and membrane hydrophilicity (*WCA*) can be ascribed to that GO exhibits abundant functional groups [20].

Further modification of GO with PEG rendered the AM-CMPSF membrane superhydrophilic, while the increased interlayer *d*-spacing between GO nanosheets promoted water permeation. For instance, the M4 membrane (with GO-PEG1000) exhibited a 9.6% greater $J_{w,0}$ value than the M3 membrane prepared with only GO. Moreover, among the GO-PEG stacked membranes, $J_{w,0}$ values increased from 14.8 L·m^{-2}·h^{-1} for the membrane M4 to 16.9 L·m^{-2}·h^{-1} for the membrane M6 as the PEG molecular weight was increased from 1000 to 20,000 g·mol^{-1}. This trend is consistent with the enlarged interlayer *d*-spacing of GO

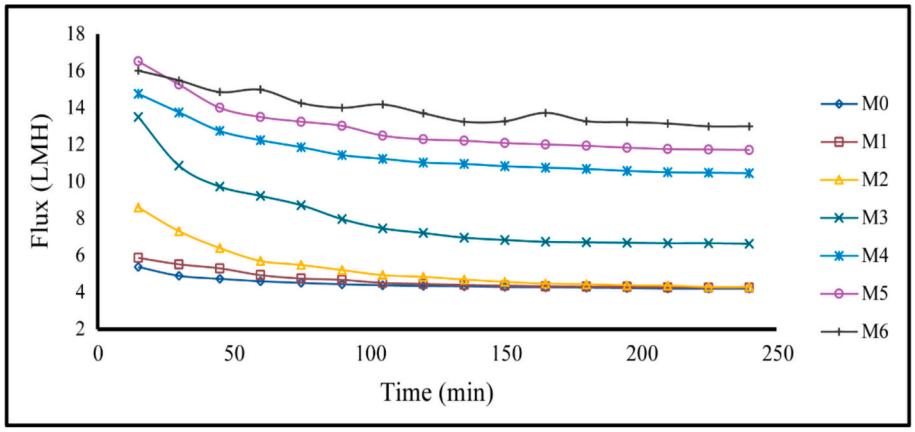

Fig. 9. Oily wastewater filtration processes of the pristine PSF membrane (M0), CMPSF membrane (M1), AM-CMPSF membrane (M2), GO stacked AM-CMPSF membrane (M3) and GO-PEG stacked AM-CMPSF membranes (M4, M5 and M6).

Table 3
Filtration performance including initial pure water flux ($J_{w,0}$), permeate flux after 4 h process (J_{oil}) for 1000 mg·L^{-1} of oil-in-water emulsion, pure water flux after fouling ($J_{w,1}$), permeate flux decline (FD_{oil}), flux recovery ratio (FRR) and oil-water relative flux reduction (RFR).

Membrane	$J_{w,0}$ (L·m^{-2}·h^{-1})	J_{oil} (L·m^{-2}·h^{-1})	$J_{w,1}$ (L·m^{-2}·h^{-1})	FD_{oil} (%)	FRR (%)	RFR (%)
M0	5.9 ± 0.9	4.2 ± 0.3	4.2 ± 1.0	21,8	71.2	28.6
M1	6.1 ± 1.4	4.3 ± 0.4	4.8 ± 2.0	27.5	78.7	30.1
M2	8.6 ± 0.8	4.3 ± 0.7	6.7 ± 1.8	50.1	77.9	50.0
M3	13.5 ± 3.2	6.6 ± 1.4	10.5 ± 2.8	50.8	77.8	50.8
M4	14.8 ± 2.9	10.5 ± 0.7	11.9 ± 2.3	29.1	80.4	29.3
M5	16.5 ± 1.0	11.7 ± 1.2	14.1 ± 3.6	29.1	85.5	28.9
M6	16.9 ± 2.6	13.0 ± 0.9	14.7 ± 2.8	18.8	87.0	23.0

nanosheets induced by PEG functionalization, as discussed previously.

Fig. 9 shows the permeate flux-time curves of all prepared membranes during filtration of 1.0 g·L^{-1} oil-in-water emulsion. The pristine PSF (M0) and CMPSF (M1) membranes exhibited nearly same permeate fluxes. Animation of CMPSF membrane (M2) improved the initial permeate flux; however, after 120 min of operation the flux decreased to levels similar to those of M0 and M1, indicating rapid fouling in the absence of a stacked GO layer. In contrast, both the initial and final fluxes of the GO and GO-PEG-modified membranes (M3–M6) were higher than those of M0–M2, confirming the role of surface-stacked GO and GO-PEG in improving antifouling performance.

PEG functionalization of GO further enhanced fouling resistance. The initial permeate fluxes of M3, M4, M5 and M6 membranes were 13.5, 14.8 and 16.5 and 16.0 L·m^{-2}·h^{-1}, respectively, which decreased after 120 min to 6.6, 10.5, 11.7 and 13.0 L·m^{-2}·h^{-1}. The permeate flux decline (FD_{oil}) values, also summarized in Table 3, give interesting information about the fouling behavior of the membranes during oily wastewater treatment. The FD_{oil} values were for both M0 and M1 (21.8% and 27.5%, respectively) indicating negligible differences between pristine PSF and chloromethylated PSF membranes in flux-time behavior using oil-in-water emulsion. In contrast, the FD_{oil} values increased markedly to ~50% for M2 and M3 membranes, whereas PEG modification reduced FD_{oil} progressively with PEG molecular weight, reaching 18.8% for M6 membrane. The improved antifouling behavior of GO-PEG membranes can be attributed to two factors: (i) the intrinsic hydrophilicity of PEG, which introduces hydroxyl groups that promote

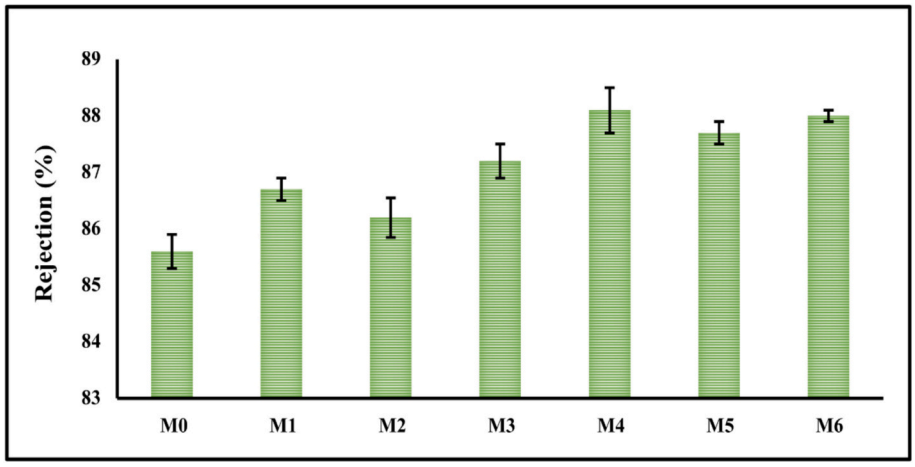

Fig. 10. Oil rejection factor of the pristine PSF membrane (M0), CMPSF membrane (M1), AM-CMPSF membrane (M2), GO stacked AM-CMPSF membrane (M3) and GO-PEG stacked AM-CMPSF membranes (M4, M5 and M6).

Table 4
Comparison of performance of membrane M6 with PSF-based membranes for oily wastewater treatment.

Membrane (weight ratio PSF/additive)	WCA (°)	Oil type (c_{oil}, mg/L)	*PWP* (L m^{-2} h^{-1} bar^{-1})	J_{oil} at TMP (L m^{-2} h^{-1})	*R* (%)	FD_{oil} (%)	*FRR* (%)	*RFR* (%)	Reference
PSF/CNT-GO (HF) 20 wt%/1 wt%	51.4	Oil + SDS (1000)	370.8	–	98.7	–	90.5	–	[38]
PSF/PEG20000 12/5	–	Crude oil (100)	375	~15 (1 bar)	92	51 (2.5 h)	–	96	[10]
PSF/bentonite 15/0.82	60	– (200)	309	44,6 (1 bar)	90	85 (5 h)	–	85.6	[77]
PSF/P(VP-AN)-g-bentonite 15/0.82	44	– (200)	400	296 (1 bar)	97	25.3 (5 h)	–	26	[77]
PSF/CNT 20/5	77,3	Diesel oil (1000)	3.2	2.5 (1.38 bar)	99,88	–	–	21.9	[36]
PSF/GO-PAMAM 17/0.8	57	QALCO® (1000)	196.3	–	99.5	–	75.6 (BSA[a])	60 (BSA[a])	[52]
PSF/ZnO 18/1	68	Petroleum refinery wastewater	–	7.1 (5 bar)	85.8	53.5 (3 h)	70.0	44.7	[32]
PSF/ZnO/PVA 18/1/3	45	Petroleum refinery wastewater	–	4.1 (5 bar)	93	0.6 (3 h)	86.5	35.6	[32]
PSF/ZnO-HNT 14/14	48.5	Hexadecane oil (250)	869	–	95	–	–	–	[78]
PSF/MOFs/PEG 15/6/5	70.8	– (100)	26.3	47.8 (2.5 bar)	97.8	34.9	78.2	32.2	[79]
PSF/PVP/GO + AA 15/5/0.2	64	Diesel (100)	1375	650 (3 bar)	97.9	90	90 (BSA[a])	–	[53]
PSF/PVP/HAO 15/1.5/30	8	Synthetic oil (1000)	1180	200 (1 bar)	~100	58.3	66.1	83.1	[37]
PSF/PEG/PTS 15/4/10	45.5	Lubricant oil (160)	210	17 (1 bar)	92	87	–	91.9	[80]
PSF/SYZ SYZ/PSF: 15%	45.2	– (80)	62.8	110 (2 bar)	99.2	53.5	–	12.4	[81]
PSF/PVP/LDH-Mt 18/5/1	7.7	Transformer oil+SDS (1000)	455	94 (1.3 bar)	87.2	~23	82.8 (BSA[a])	84.1	[82]
PSF/PVP/MNPs 18/5.4/1.5	64.2	– (50)	153.4	–	46.5	–	91	–	[83]
PSF/PEG/SiO_2NPs -/10% of PSF/10% of PSF	65.8	Machine oil (65)	232	60 (0.5 bar)	98.7	56.2	–	48.3	[84]
PSF/PVP/PP/FOTS-SiO_2NPs 15/0.16/3/0.15	89	Motor engine oil (–)	87	75.5	83.4	–	–	13.2	[85]
PSF/PVP 8.75/8.25	53.6	Vegetable oil+SDS (2000)	30.1	33.6 (2 bar)	92.7	27.2	69.7	44.3	[86]
PSF/PEG 8.75/8.25	66	Vegetable oil+SDS (2000)	32	4.7 (2 bar)	91.4	30.4	75.5	92.7	[86]
PSF/GO-PEG20000 14/0.1	<10	Vegetable oil+SDS (1000)	11.3	13 (1.5 bar)	88	18.8	87	23	M6 in this study

CNT: carbon nanotubes; HF: hollow fiber membranes; SDS: sodium lauryl sulphate; P(VP-AN): poly(1-vinylpyrrolidone-*co*-acrylonitrile); PAMAM: poly(amido amine); BSA: bovine serum albumin; PVA: polyvinyl alcohol; ZnO: zinc oxide; ZnO-HNT: zinc oxide-Halloysite nanotubes; MOFs: metal-organic frameworks (UiO-66-$(COOH)_2$); AA: aspartic acid; HAO: inorganic hydrous aluminum oxide; PTS: phosphorylated TiO_2–SiO_2; SZY: sulfated Y-doped zirconia; PVP: polyvinylpyrrolidone; LDH-Mt: Mg-Fe layered double hydroxide modified montmorillonite; MNPs: magnetic nanoparticles; SiO_2NPs: modified silica nanoparticles; FOTS-SiO2NPs: 1H, 1H, 2H, 2H-perfluorooctyltriethoxysilane modified SiO_2NPs.

[a] Fouling experiment was conducted with BSA.

water adsorption and repel oil droplets; and (ii) the increased interlayer *d*-spacing of GO nanochannels at higher PEG molecular weights, which facilitates water permeation through the stacked top layer of this type of membranes (M4, M5 and M6) enhanced in comparison to the membrane M3. Moreover, the presence of PEG chains on the membrane surface hinder oil adsorption due to steric repulsion and polarity mismatch with non-polar oil droplets. This effect is more pronounced with longer PEG chains, as evidenced by the lower flux decline of M6 (18.8%) compared to M4 (50.8%). Overall, the results confirm that surface fouling is the primary cause of flux decline, and that PEG functionalization of GO layers significantly mitigates this effect.

The oil-water separation performance of all prepared membranes was evaluated, and the results are presented in Table 3. To evaluate the oil-fouling resistance of the membranes, flux recovery ratio (*FRR*) and oil-water relative flux reduction (*RFR*) were calculated from Eqs. (7) and (8), respectively. The *FFR* values summarized in Table 3 reveal that the pristine PSF membrane (M0) exhibited the lowest flux recovery ratio, whereas the GO-PEG modified membrane with the highest PEG molecular weight (M6) displayed the highest (*FRR* of 87%). The incorporation of GO and GO-PEG layers on the surface of AM-CMPSF membranes markedly reduced the fouling tendency. Since membrane fouling is strongly influenced by hydrophilicity, hydrophilic and superhydrophilic surfaces are generally less prone to foul [74–76]. In this study, both the GO and GO-PEG top layers on AM-CMPSF membrane surfaces exhibited a superhydrophilic behavior, as previously demonstrated. It must be pointed out that increasing the PEG molecular weight further improved antifouling performance, which can be attributed to stronger repulsive interactions between longer PEG chains and oil droplets, thereby inhibiting oil deposition on the membrane surface. Similar trend to flux decline was observed for oil-water relative flux reduction, *RFR*, obtaining the lowest oil-water flux reduction (23%) for the M6 membranes. The deposition of GO and GO-PEG layers on AM-CMPSF membranes substantially decreased fouling tendency, thereby limiting their oil adsorption on the membrane surface.

The oil rejection factor (*R*) of the membranes is shown in Fig. 10. Both GO and GO-PEG stacked membranes showed slightly higher oil rejection factors, *R*, compared to the pristine PSF (M0), CMPSF (M1), and AM-CMPSF (M2) membranes confirming that the incorporation of GO-based and GO-PEG-based layers not only enhanced permeate flux but also improved oil rejection. As mentioned previously, this

improvement is consistent with the capillary-driven water transport through GO/GO-PEG nanosheets, which promotes selective water permeation while restricting oil transport. In addition, the presence of hydrophilic PEG chains on the membrane surface facilitates the formation of a hydrated barrier layer, further hindering oil droplet deposition and penetration.

Table 4 compares the performance of membrane M6 with other polysulfone-based membranes in terms of pure water permeability, (*PWP*, $L{\cdot}m^{-2}{\cdot}h^{-1}{\cdot}bar^{-1}$), permeate flux ($J_{oil}$) for oily wastewater treatment and its oil rejection factor (*R*), as well as fouling performance like permeate flux decline (FD_{oil}), flux recovery ratio (*FRR*) and oil-water relative flux reduction (*RFR*). Membrane M6 exhibited a lower *PWP* value than most membranes reported in the literature; however, its oil rejection factor was comparable to those of previously published PSF-based membranes. The antifouling performance of membrane M6 represents the most notable outcome of this study, being considerably higher than values previously reported in literature. This is reflected in the lowest FD_{oil} value (18.8%), together with a remarkably high *FFR* (87%) and an oil-water relative flux reduction, *RFR*, low (23%). These excellent antifouling characteristics are attributed to the presence of GO-PEG layer deposited on the PSF substrate, as previously highlighted.

4. Conclusions

In this study, effects of graphene oxide (GO) and polyethylene glycol-functionalized GO (GO-PEG) on the surface properties of polysulfone (PSF) membranes were systematically investigated for oily wastewater treatment. The key findings are summarized as follows:

Increasing the PEG molecular weight expanded the interlayer d-spacing of GO nanosheets, as evidenced by the XRD peak shift from 9.47° for GO-PEG1000 to 9.19° for GO-PEG20000. The tensile strength also increased, from 5.12 MPa for the neat PSF membrane to 6.12 MPa for the membrane containing GO-PEG20000, due to enhanced interfacial interactions between GO-PEG and the polymer matrix.

The incorporation of GO and GO-PEG layers rendered the water contact angle became unmeasurable owing to rapid droplet absorption, indicating a significant increase in surface hydrophilicity. Moreover, water uptake increased from 30.6% for the neat PSF membrane (M0) to 84.6% for the GO-PEG20000 modified membrane (M6), largely attributed to capillary-driven transport through GO and GO-PEG derived nanochannels.

Filtration tests using a 1000 mg/L oil-in-water emulsion revealed notable enhancements in permeate flux and fouling resistance. The initial pure water flux increased from 5.9 $L{\cdot}m^{-2}{\cdot}h^{-1}$ for the membrane M0 to 16.9 $L{\cdot}m^{-2}{\cdot}h^{-1}$ for the membrane M6, while oil rejection remained consistently high across all membranes (85.6–88.1%).

GO and GO-PEG stacked membranes exhibited superior fouling resistance compared to pristine PSF, CMPSF, and AM-CMPSF membranes, with a decrease of the irreversible fouling ratio (IFR) from 28.6% for to 23.0%. The incorporation of longer PEG chains not only facilitated water transport via increased interlayer spacing but also introduced polar functional groups that effectively repelled non-polar oil droplets.

Overall, these results highlight the potential of GO-PEG modified membranes as a robust and scalable solution for fabricating super-hydrophilic, fouling-resistant membranes tailored for advanced oily wastewater treatment.

Supplementary data to this article can be found online at https://doi.org/10.1016/j.jwpe.2026.109479.

CRediT authorship contribution statement

Y. Jafarzadeh: Writing – original draft, Validation, Methodology, Investigation, Formal analysis, Data curation. **C. García-Payo:** Writing – review & editing, Methodology, Formal analysis. **M. Khayet:** Writing – review & editing, Visualization, Validation, Supervision, Resources, Project administration, Methodology, Investigation, Funding acquisition, Formal analysis, Data curation.

Declaration of competing interest

The authors declare that they have no known competing financial interests or personal relationships that could have appeared to influence the work reported in this paper.

Acknowledgments

This publication is part of project PID2022-138389OB-C31, funded by MICIU/AEI/10.13039/501100011033/FEDER, UE.

Data availability

Data will be made available on request.

References

[1] W. Tomczak, M. Gryta, Application of ultrafiltration ceramic membrane for separation of oily wastewater generated by maritime transportation, Sep. Purif. Technol. 261 (2021) 118259, https://doi.org/10.1016/j.seppur.2020.118259.
[2] X. Zhu, W. Tu, K.-H. Wee, R. Bai, Effective and low fouling oil/water separation by a novel hollow fiber membrane with both hydrophilic and oleophobic surface properties, J. Membr. Sci. 466 (2014) 36–44, https://doi.org/10.1016/j.memsci.2014.04.038.
[3] T. Ahmad, C. Guria, A. Mandal, A review of oily wastewater treatment using ultrafiltration membrane: a parametric study to enhance the membrane performance, J. Water Process Eng. 36 (2020) 101289, https://doi.org/10.1016/j.jwpe.2020.101289.
[4] A.H. Behroozi, M.R. Ataabadi, Improvement in microfiltration process of oily wastewater: a comprehensive review over two decades, J. Environ. Chem. Eng. 9 (1) (2021), https://doi.org/10.1016/j.jece.2020.104981.
[5] N.H. Ismail, W.N.W. Salleh, A.F. Ismail, H. Hasbullah, N. Yusof, F. Aziz, J. Jaafar, Hydrophilic polymer-based membrane for oily wastewater treatment: a review, Sep. Purif. Technol. 233 (2020), https://doi.org/10.1016/j.seppur.2019.116007.
[6] O. Samuel, M.H.D. Othman, R. Kamaludin, T.A. Kurniawan, T. Li, H. Dzinun, A. Imtiaz, Treatment of oily wastewater using photocatalytic membrane reactors: a critical review, J. Environ. Chem. Eng. 10 (6) (2022) 108539, https://doi.org/10.1016/j.jece.2022.108539.
[7] F. Fotovat, M. Hosseini, Treatment of oily wastewater by electrocoagulation: simultaneous optimization of oil removal efficiency and specific energy consumption, J. Water Process Eng. 55 (2023) 104221, https://doi.org/10.1016/j.jwpe.2023.104221.
[8] S. Huang, R.H.A. Ras, X. Tian, Antifouling membranes for oily wastewater treatment: interplay between wetting and membrane fouling, Curr. Opin. Colloid Interface Sci. 36 (2018) 90–109, https://doi.org/10.1016/j.cocis.2018.02.002.
[9] T.D. Kusworo, D.P. Utomo Qudratun, Performance evaluation of double stage process using nano hybrid PES/SiO2-PES membrane and PES/ZnO-PES membranes for oily waste water treatment to clean water, J. Environ. Chem. Eng. 5 (6) (2017) 6077–6086, https://doi.org/10.1016/j.jece.2017.11.044.
[10] B. Chakrabarty, A.K. Ghoshal, M.K. Purkait, Ultrafiltration of stable oil-in-water emulsion by polysulfone membrane, J. Membr. Sci. 325 (1) (2008) 427–437, https://doi.org/10.1016/j.memsci.2008.08.007.
[11] M. Manouchehri, A comprehensive review on state-of-the-art antifouling super (wetting and anti-wetting) membranes for oily wastewater treatment, Adv. Colloid Interf. Sci. 323 (2024) 103073, https://doi.org/10.1016/j.cis.2023.103073.
[12] P. Arribas, M.C. García-Payo, M. Khayet, L. Gil, Improved antifouling performance of polyester thin film nanofiber composite membranes prepared by interfacial polymerization, J. Membr. Sci. 598 (2020) 117774, https://doi.org/10.1016/j.memsci.2019.117774.
[13] A. Behboudi, Y. Jafarzadeh, R. Yegani, Polyvinyl chloride/polycarbonate blend ultrafiltration membranes for water treatment, J. Membr. Sci. 534 (2017) 18–24, https://doi.org/10.1016/j.memsci.2017.04.011.
[14] N.F. Zulkefli, N.H. Alias, N.S. Jamaluddin, N. Abdullah, S.F. Abdul Manaf, N. H. Othman, F. Marpani, M.S. Mat-Shayuti, T.D. Kusworo, Recent mitigation strategies on membrane fouling for oily wastewater treatment, Membranes (Basel) 12 (1) (2021), https://doi.org/10.3390/membranes12010026.
[15] H. Nagasawa, T. Omura, T. Asai, M. Kanezashi, T. Tsuru, Filtration of surfactant-stabilized oil-in-water emulsions with porous ceramic membranes: effects of membrane pore size and surface charge on fouling behavior, J. Membr. Sci. 610 (2020) 118210, https://doi.org/10.1016/j.memsci.2020.118210.
[16] M.A. Kivi, H. Alinia, Y. Jafarzadeh, R. Yegani, High-density polyethylene membranes embedded with carboxylated and polyethylene glycol-grafted nanodiamond to be used in membrane bioreactors, J. Appl. Polym. Sci. 136 (35) (2019) 47914, https://doi.org/10.1002/app.47914.
[17] M. Yang, P. Hadi, X. Yin, J. Yu, X. Huang, H. Ma, H. Walker, B.S. Hsiao, Antifouling nanocellulose membranes: how subtle adjustment of surface charge lead to self-cleaning property, J. Membr. Sci. 618 (2021) 118739, https://doi.org/10.1016/j.memsci.2020.118739.

[18] Y.-Y. Su, X. Yan, Y. Chen, X.-J. Guo, X.-F. Chen, W.-Z. Lang, Facile fabrication of COF-LZU1/PES composite membrane via interfacial polymerization on microfiltration substrate for dye/salt separation, J. Membr. Sci. 618 (2021) 118706, https://doi.org/10.1016/j.memsci.2020.118706.
[19] F. Beygmohammdi, H. Nourizadeh Kazerouni, Y. Jafarzadeh, H. Hazrati, R. Yegani, Preparation and characterization of PVDF/PVP-GO membranes to be used in MBR system, Chem. Eng. Res. Des. 154 (2020) 232–240, https://doi.org/10.1016/j.cherd.2019.12.016.
[20] S. Khakpour, Y. Jafarzadeh, R. Yegani, Incorporation of graphene oxide/nanodiamond nanocomposite into PVC ultrafiltration membranes, Chem. Eng. Res. Des. 152 (2019) 60–70, https://doi.org/10.1016/j.cherd.2019.09.029.
[21] Y. Jafarzadeh, R. Yegani, M. Sedaghat, Preparation, characterization and fouling analysis of ZnO/polyethylene hybrid membranes for collagen separation, Chem. Eng. Res. Des. 94 (2015) 417–427, https://doi.org/10.1016/j.cherd.2014.08.017.
[22] T.A. Makhetha, R.M. Moutloali, Incorporation of a novel Ag–Cu@ZIF-8@GO nanocomposite into polyethersulfone membrane for fouling and bacterial resistance, J. Membr. Sci. 618 (2021) 118733, https://doi.org/10.1016/j.memsci.2020.118733.
[23] R. Chen, L. Mao, C.N. Matindi, G. Liu, J. He, Z. Cui, X. Ma, K. Fang, B. Wu, B. B. Mamba, J. Li, Tailoring the micro-structure of PVC/SMA-g-PEG blend ultrafiltration membrane with simultaneously enhanced hydrophilicity and toughness by in situ reaction-controlled phase inversion, J. Membr. Sci. 653 (2022) 120545, https://doi.org/10.1016/j.memsci.2022.120545.
[24] V. Shah, B. Wang, K. Li, Blending modification to porous polyvinylidene fluoride (PVDF) membranes prepared via combined crystallisation and diffusion (CCD) technique, J. Membr. Sci. 618 (2021) 118708, https://doi.org/10.1016/j.memsci.2020.118708.
[25] Y. Deng, G. Zhang, R. Bai, S. Shen, X. Zhou, I. Wyman, Fabrication of superhydrophilic and underwater superoleophobic membranes via an in situ crosslinking blend strategy for highly efficient oil/water emulsion separation, J. Membr. Sci. 569 (2019) 60–70, https://doi.org/10.1016/j.memsci.2018.09.069.
[26] K. Eum, D.W. Kim, Y. Choi, X. Duan, M.A. Hillmyer, M. Tsapatsis, Assembly of graphene oxide nanosheets on diamine-treated pvdf hollow fiber as nanofiltration membranes, ACS Appl. Polym. Mater. 2 (9) (2020) 3859–3866, https://doi.org/10.1021/acsapm.0c00558.
[27] M. Hu, B. Mi, Enabling graphene oxide nanosheets as water separation membranes, Environ. Sci. Technol. 47 (8) (2013) 3715–3723, https://doi.org/10.1021/es400571g.
[28] M. Hu, B. Mi, Layer-by-layer assembly of graphene oxide membranes via electrostatic interaction, J. Membr. Sci. 469 (2014) 80–87, https://doi.org/10.1016/j.memsci.2014.06.036.
[29] O.S. Serbanescu, S.I. Voicu, V.K. Thakur, Polysulfone functionalized membranes: properties and challenges, Mater. Today Chem. 17 (2020) 100302, https://doi.org/10.1016/j.mtchem.2020.100302.
[30] A. Tizchang, Y. Jafarzadeh, R. Yegani, S. Khakpour, The effects of pristine and silanized nanodiamond on the performance of polysulfone membranes for wastewater treatment by MBR system, J. Environ. Chem. Eng. 7 (6) (2019) 103447, https://doi.org/10.1016/j.jece.2019.103447.
[31] S.M. Abbas, S.M. Al-Jubouri, High performance and antifouling zeolite@polyethersulfone/cellulose acetate asymmetric membrane for efficient separation of oily wastewater, J. Environ. Chem. Eng. 12 (3) (2024) 112775, https://doi.org/10.1016/j.jece.2024.112775.
[32] T.D. Kusworo, A.C. Kumoro, N. Aryanti, D.P. Utomo, H. Qoyyimah, S.R. Alexandro Hasbullah, Effects of crosslinking and thermal annealing modifications on the performance of nanohybrid PSf-ZnO membranes for the treatment of raw and ozonated petroleum refinery wastewater, J. Environ. Chem. Eng. 9 (5) (2021), https://doi.org/10.1016/j.jece.2021.106200.
[33] V. Yadav, S.K. Raj, N.H. Rathod, V. Kulshrestha, Polysulfone/graphene quantum dots composite anion exchange membrane for acid recovery by diffusion dialysis, J. Membr. Sci. 611 (2020) 118331, https://doi.org/10.1016/j.memsci.2020.118331.
[34] S.S. Alias, Z. Harun, M.F. Shohur, Effect of monovalent and divalent ions in non-solventcoagulation bath-induced phase inversionon the characterization of a porous polysulfone membrane, Polym. Bull. 76 (2019) 5957–5979, https://doi.org/10.1007/s00289-019-02689-z.
[35] T.V. Plisko, A.V. Bildyukevich, K.S. Burts, T.A. Hliavitskaya, A.V. Penkova, S. S. Ermakov, M. Ulbricht, Modification of polysulfone ultrafiltration membranes via addition of anionic polyelectrolyte based on acrylamide and sodium acrylate to the coagulation bath to improve antifouling performance in water treatment, Membranes 10 (10) (2020) 264.
[36] M.O. Daramola, P. Hlanyane, O.O. Sadare, O.O. Oluwasina, S.E. Iyuke, Performance of carbon nanotube/polysulfone (CNT/Psf) composite membranes during oil-water mixture separation: effect of CNT dispersion method, Membranes (Basel) 7 (1) (2017), https://doi.org/10.3390/membranes7010014.
[37] R. Jamshidi Gohari, F. Korminouri, W.J. Lau, A.F. Ismail, T. Matsuura, M.N. K. Chowdhury, E. Halakoo, M.S. Jamshidi Gohari, A novel super-hydrophilic PSf/HAO nanocomposite ultrafiltration membrane for efficient separation of oil/water emulsion, Sep. Purif. Technol. 150 (2015) 13–20, https://doi.org/10.1016/j.seppur.2015.06.031.
[38] A. Modi, J. Bellare, Efficiently improved oil/water separation using high flux and superior antifouling polysulfone hollow fiber membranes modified with functionalized carbon nanotubes/graphene oxide nanohybrid, J. Environ. Chem. Eng. 7 (2) (2019), https://doi.org/10.1016/j.jece.2019.102944.
[39] A. Avornyo, C.V. Chrysikopoulos, Applications of graphene oxide (GO) in oily wastewater treatment: recent developments, challenges, and opportunities, J. Environ. Manag. 353 (2024) 120178, https://doi.org/10.1016/j.jenvman.2024.120178.
[40] Q. Guo, M. Xu, Q. Tang, Y. Liu, W. Zhang, C. Guo, X. Zhao, Y. Zhu, S. Ye, D. Liu, W. Lei, C. Chen, Advanced hybrid nanosheet membranes with stable nanochannels for ultrafast molecular separation, npj Clean Water 6 (1) (2023) 38, https://doi.org/10.1038/s41545-023-00250-0.
[41] S.C. Ray, Chapter 2 - application and uses of graphene oxide and reduced graphene oxide, in: S.C. Ray (Ed.), Applications of Graphene and Graphene-oxide Based Nanomaterials, William Andrew Publishing, Oxford, 2015, pp. 39–55, https://doi.org/10.1016/B978-0-323-37521-4.00002-9.
[42] R. Rashidi, S. Khakpour, S. Masoumi, Y. Jafarzadeh, Effects of GO-PEG on the performance and structure of PVC ultrafiltration membranes, Chem. Eng. Res. Des. 177 (2022) 815–825, https://doi.org/10.1016/j.cherd.2021.11.021.
[43] Y. Wei, Q. Liu, Q. Lian, Y. Wang, Y. Zhu, P. Zhang, B. Wang, Insight into the separation mechanism of graphene oxide membrane by designing dual layered structure, Desalination 532 (2022) 115687, https://doi.org/10.1016/j.desal.2022.115687.
[44] Q. Huang, S. Zhang, X. Li, Y. Wu, Y. Liu, J. Ran, P. Cui, C.-F. Fu, L. Ding, T. Xu, Intelligent graphene oxide membranes with pH tunable channels for water treatment, Chem. Eng. J. 431 (2022) 133462, https://doi.org/10.1016/j.cej.2021.133462.
[45] M. Zare, M. Rahbari-Sisakht, A. Mansourizadeh, Anti-fouling polysulfone-graphene oxide ultrafiltration membrane with high capability in water/oil emulsion separation, J. Clust. Sci. 35 (8) (2024) 2787–2802, https://doi.org/10.1007/s10876-024-02695-w.
[46] M. Zubair, S. Farooq, A. Hussain, S. Riaz, A. Ullah, A review of current developments in graphene oxide–polysulfone derived membranes for water remediation, Environ. Sci. Adv. 3 (7) (2024) 983–1003, https://doi.org/10.1039/d4va00058g.
[47] H. Jiang, J.-H. Liu, X. Chen, X. Cao, X. Ye, G. Shi, Highly efficient separation of Sc3 + and Y3+ in acid solution by a graphene oxide membrane with interlayer sieving, J. Rare Earths (2024), https://doi.org/10.1016/j.jre.2024.02.017.
[48] W. Geng, Z. Zhang, Q. Guo, Y. Liu, X. Ye, H. Zhang, C. Fu, F. Liu, Y. Zhu, C. Chen, Tailoring graphene oxide nanofiltration membrane with adjustable nanochannels for enhanced molecule separation, Chem. Eng. J. 478 (2023) 147327, https://doi.org/10.1016/j.cej.2023.147327.
[49] W. Geng, C. Cheng, B. Ge, Y. Xu, Y. Liu, X. Ye, C. Huang, W. Lei, Y. Wang, D. Sun, C. Chen, Charge-selective nanoconfined boron nitride membranes for ultrafast and enhanced water decontamination, Adv. Membr. 5 (2025) 100159, https://doi.org/10.1016/j.advmem.2025.100159.
[50] A. Alkhouzaam, H. Qiblawey, Novel polysulfone ultrafiltration membranes incorporating polydopamine functionalized graphene oxide with enhanced flux and fouling resistance, J. Membr. Sci. 620 (2021) 118900, https://doi.org/10.1016/j.memsci.2020.118900.
[51] A.T. Yasir, A. Benamor, A.H. Hawari, Enhancement of polysulfone ultrafiltration membrane with third generation poly(amido amine)-graphene oxide nanocomposite, J. Water Process Eng. 54 (2023), https://doi.org/10.1016/j.jwpe.2023.103991.
[52] A.T. Yasir, A. Benamor, M. Ba-Abbad, A.H. Hawari, Performance of polysulfone ultrafiltration membranes incorporating graphene oxide nanoparticles functionalized with different generations of poly(amido amine), J. Water Process Eng. 60 (2024), https://doi.org/10.1016/j.jwpe.2024.105095.
[53] O. Abdalla, M.A. Wahab, A. Abdala, Mixed matrix membranes containing aspartic acid functionalized graphene oxide for enhanced oil-water emulsion separation, J. Environ. Chem. Eng. 8 (5) (2020), https://doi.org/10.1016/j.jece.2020.104269.
[54] H. Wang, W. Wang, L. Wang, B. Zhao, Z. Zhang, X. Xia, H. Yang, Y. Xue, N. Chang, Enhancement of hydrophilicity and the resistance for irreversible fouling of polysulfone (PSF) membrane immobilized with graphene oxide (GO) through chloromethylated and quaternized reaction, Chem. Eng. J. 334 (2018) 2068–2078, https://doi.org/10.1016/j.cej.2017.11.135.
[55] J. Ren, Y. Dong, J. Dai, H. Hu, Y. Zhu, X. Teng, A novel chloromethylated/quaternized poly(sulfone)/poly(vinylidene fluoride) anion exchange membrane with ultra-low vanadium permeability for all vanadium redox flow battery, J. Membr. Sci. 544 (2017) 186–194, https://doi.org/10.1016/j.memsci.2017.09.015.
[56] O. Dumbrava, A. Filimon, L. Marin, Tailoring properties and applications of polysulfone membranes by chemical modification: structure-properties-applications relationship, Eur. Polym. J. 196 (2023), https://doi.org/10.1016/j.eurpolymj.2023.112316.
[57] F. Moghadam, T.H. Lee, I. Park, H.B. Park, Thermally annealed polyimide-based mixed matrix membrane containing ZIF-67 decorated porous graphene oxide nanosheets with enhanced propylene/propane selectivity, J. Membr. Sci. 603 (2020) 118019, https://doi.org/10.1016/j.memsci.2020.118019.
[58] S. Mohammadi, A. Babaei, Poly (vinyl alcohol)/chitosan/polyethylene glycol-assembled graphene oxide bio-nanocomposites as a prosperous candidate for biomedical applications and drug/food packaging industry, Int. J. Biol. Macromol. 201 (2022) 528–538, https://doi.org/10.1016/j.ijbiomac.2022.01.086.
[59] Y. Liu, J. Wang, Preparation of anion exchange membrane by efficient functionalization of polysulfone for electrodialysis, J. Membr. Sci. 596 (2020) 117591, https://doi.org/10.1016/j.memsci.2019.117591.
[60] X. Lin, S. Kim, D.M. Zhu, E. Shamsaei, T. Xu, X. Fang, H. Wang, Preparation of porous diffusion dialysis membranes by functionalization of polysulfone for acid recovery, J. Membr. Sci. 524 (2017) 557–564, https://doi.org/10.1016/j.memsci.2016.11.059.

[61] X. Tian, Y.-R. Qiu, 2-methoxyethylacrylate modified polysulfone membrane and its blood compatibility, Arch. Biochem. Biophys. 631 (2017) 49–57, https://doi.org/10.1016/j.abb.2017.07.018.
[62] X. Li, H.-b. Sun, X. Sun, Polysulfone grafted with anthraquinone-hydroanthraquinone redox as a flexible membrane electrode for aqueous batteries, Polymer 234 (2021) 124245, https://doi.org/10.1016/j.polymer.2021.124245.
[63] C. Wang, N. Pan, Y. Jiang, J. Liao, A. Sotto, H. Ruan, C. Gao, J. Shen, A facile approach to prepare crosslinked polysulfone-based anion exchange membranes with enhanced alkali resistance and dimensional stability, RSC Adv. 9 (62) (2019) 36374–36385, https://doi.org/10.1039/C9RA07433C.
[64] P. Arribas, M. Khayet, M.C. García-Payo, L. Gil, Self-sustained electro-spun polysulfone nano-fibrous membranes and their surface modification by interfacial polymerization for micro- and ultra-filtration, Sep. Purif. Technol. 138 (2014) 118–129, https://doi.org/10.1016/j.seppur.2014.10.010.
[65] M.N.A. Seman, M. Khayet, N. Hilal, Nanofiltration thin-film composite polyester polyethersulfone-based membranes prepared by interfacial polymerization, J. Membr. Sci. 348 (1) (2010) 109–116, https://doi.org/10.1016/j.memsci.2009.10.047.
[66] F. Fayyazi, E. Ahmadi Feijani, H. Mahdavi, Chemically modified polysulfone membrane containing palladium nanoparticles: preparation, characterization and application as an efficient catalytic membrane for Suzuki reaction, Chem. Eng. Sci. 134 (2015) 549–554, https://doi.org/10.1016/j.ces.2015.05.008.
[67] Y. Li, M. Li, S. Zhou, A. Xue, Y. Zhang, Y. Zhao, J. Zhong, Q. Zhang, D. Yang, Enhancement of hydroxide conductivity by incorporating nanofiber-like palygorskite into quaternized polysulfone as anion exchange membranes, Appl. Clay Sci. 195 (2020) 105702, https://doi.org/10.1016/j.clay.2020.105702.
[68] M.S. Jyothi, V. Nayak, M. Padaki, R. Geetha Balakrishna, K. Soontarapa, Aminated polysulfone/TiO2 composite membranes for an effective removal of Cr(VI), Chem. Eng. J. 283 (2016) 1494–1505, https://doi.org/10.1016/j.cej.2015.08.116.
[69] A. Behboudi, Y. Jafarzadeh, R. Yegani, Preparation and characterization of TiO2 embedded PVC ultrafiltration membranes, Chem. Eng. Res. Des. 114 (2016) 96–107, https://doi.org/10.1016/j.cherd.2016.07.027.
[70] M.M. Khosroshahi, Y. Jafarzadeh, M. Nasiri, M. Khayet, Novel polyvinyl chloride ultrafiltration membranes blended with amphiphilic polyethylene glycol-block-poly(1, 2-dichloroethylene) copolymer for oily wastewater treatment, J. Water Process Eng. 56 (2023) 104433, https://doi.org/10.1016/j.jwpe.2023.104433.
[71] Y. Zhang, Q. Zhang, D. Hou, J. Zhang, Tuning interfacial structure and mechanical properties of graphene oxide sheets/polymer nanocomposites by controlling functional groups of polymer, Appl. Surf. Sci. 504 (2020) 144152, https://doi.org/10.1016/j.apsusc.2019.144152.
[72] S. Singh, A.M. Varghese, K.S.K. Reddy, G.E. Romanos, G.N. Karanikolos, Polysulfone mixed-matrix membranes comprising poly(ethylene glycol)-grafted carbon nanotubes: mechanical properties and CO2 separation performance, Ind. Eng. Chem. Res. 60 (30) (2021) 11289–11308, https://doi.org/10.1021/acs.iecr.1c02040.
[73] W.-S. Hung, C.-H. Tsou, M. De Guzman, Q.-F. An, Y.-L. Liu, Y.-M. Zhang, C.-C. Hu, K.-R. Lee, J.-Y. Lai, Cross-linking with diamine monomers to prepare composite graphene oxide-framework membranes with varying d-spacing, Chem. Mater. 26 (9) (2014) 2983–2990, https://doi.org/10.1021/cm5007873.
[74] L. Shapouri, S. Masoumi, N. Dadgar, Y. Jafarzadeh, Preparation, characterization, and fouling analysis of PVC/ND-PEG ultrafiltration membranes for whey separation, Diam. Relat. Mater. 142 (2024) 110776, https://doi.org/10.1016/j.diamond.2023.110776.
[75] A. Omidvar, S. Masoumi, M. Monsefi, Y. Jafarzadeh, M. Nasiri, H. Hazrati, PVC/PMMA blend ultrafiltration membranes for oil-in-water emulsion separation, Polym. Bull. 80 (8) (2023) 9275–9295, https://doi.org/10.1007/s00289-022-04514-6.
[76] A. Behboudi, T. Mohammadi, M. Ulbricht, High performance antibiofouling hollow fiber polyethersulfone nanocomposite membranes incorporated with novel surface-modified silver nanoparticles suitable for membrane bioreactor application, J. Ind. Eng. Chem. 119 (2023) 298–314, https://doi.org/10.1016/j.jiec.2022.11.049.
[77] S. Kumar, A. Mandal, C. Guria, Synthesis, characterization and performance studies of polysulfone and polysulfone/polymer-grafted bentonite based ultrafiltration membranes for the efficient separation of oil field oily wastewater, Process. Saf. Environ. Prot. 102 (2016) 214–228, https://doi.org/10.1016/j.psep.2016.03.011.
[78] S.N. Ikhsan, N. Yusof, F. Aziz, A. Ismail, Facile synthesis and characterization of Zno-HNT additive for enhancement of polysulfone membrane for Oil-In-Water separation, Mater. Today Proc. 46 (2021) 1978–1982, https://doi.org/10.1016/j.matpr.2021.02.589.
[79] D.B. Kanzariya, S. Vala, S.S. Jampa, M.K. Sinha, T.K. Pal, Synthesis of enhanced hydrophilic UiO-66-(COOH)2/PSF hybrid membrane for efficient separation of o/w and removal of water pollutants, J. Environ. Chem. Eng. 11 (5) (2023), https://doi.org/10.1016/j.jece.2023.111049.
[80] Y. Zhang, F. Liu, Y. Lu, L. Zhao, L. Song, Investigation of phosphorylated TiO2–SiO2 particles/polysulfone composite membrane for wastewater treatment, Desalination 324 (2013) 118–126, https://doi.org/10.1016/j.desal.2013.06.007.
[81] Y. Zhang, X. Shan, Z. Jin, Y. Wang, Synthesis of sulfated Y-doped zirconia particles and effect on properties of polysulfone membranes for treatment of wastewater containing oil, J. Hazard. Mater. 192 (2) (2011) 559–567, https://doi.org/10.1016/j.jhazmat.2011.05.058.
[82] D. Makwana, V. Polisetti, J. Castaño, P. Ray, H.C. Bajaj, Mg-Fe layered double hydroxide modified montmorillonite as hydrophilic nanofiller in polysulfone-polyvinylpyrrolidone blend ultrafiltration membranes: separation of oil-water mixture, Appl. Clay Sci. 192 (2020) 105636, https://doi.org/10.1016/j.clay.2020.105636.
[83] A. Bedar, D. Yadav, S. Kirti, R.K. Das, S. Saxena, S. Shukla, Nanomagnets doped antifouling membrane for fine emulsion separation, Polymer 290 (2024), https://doi.org/10.1016/j.polymer.2023.126484.
[84] Y. Zhang, L. Shan, Z. Tu, Y. Zhang, Preparation and characterization of novel Ce-doped nonstoichiometric nanosilica/polysulfone composite membranes, Sep. Purif. Technol. 63 (1) (2008) 207–212, https://doi.org/10.1016/j.seppur.2008.05.015.
[85] L. Tjale, H. Richards, O. Mahlangu, L.N. Nthunya, Silica nanoparticle modified polysulfone/polypropylene membrane for separation of oil-water emulsions, Results Eng. 16 (2022), https://doi.org/10.1016/j.rineng.2022.100623.
[86] A. Pagidi, R. Saranya, G. Arthanareeswaran, A.F. Ismail, T. Matsuura, Enhanced oil–water separation using polysulfone membranes modified with polymeric additives, Desalination 344 (2014) 280–288, https://doi.org/10.1016/j.desal.2014.03.033.